High-Resolution Profiles of Gamma-Ray Lines from the X-Class Solar Flare of 23 July, 2002

D. M. Smith[1], G. H. Share[2], R. J. Murphy[2], R. P. Lin[1,3], R. A. Schwartz[4,5], A. Y. Shih[1,3]

ABSTRACT

The *Reuven Ramaty High Energy Solar Spectroscopy Imager (RHESSI)* has produced the first high-resolution measurement of nuclear de-excitation lines in a solar flare. The flare, which occurred on 23 July, 2002, was a GOES X4.8 event at a heliocentric angle of $\sim 73^{\rm o}$. Doppler shifts and broadening are seen in lines of neon, magnesium, silicon, iron, carbon and oxygen. We compare the observed redshifts and widths to simulations with four adjustable parameters: spectral index, α/proton ratio, the angle of the line of sight to the magnetic field, and a measure of the pitch angle distribution of the accelerated ions. In all cases, the observed redshifts are greater than would be expected from models of pitch-angle scattering in a loop perpendicular to the solar surface. Either the loop containing the ions in this flare was bent toward the solar surface, or else the ions were strongly beamed along the field.

Subject headings: Sun:flares — Sun:X-rays, gamma rays — line:profiles — gamma rays:observations

1. Introduction

We report the first measurements at high energy resolution of nuclear de-excitation lines in a solar flare. These data, taken with the *Reuven Ramaty High Energy Solar Spectroscopic Imager (RHESSI),* are from the GOES X4.8-class solar flare of 23 July, 2002.

---

[1]Space Sciences Laboratory, University of California, Berkeley, Berkeley, CA 94720

[2]E. O. Hulbert Center for Space Research, Naval Research Laboratory, Washington, DC 20375

[3]Department of Physics, University of California, Berkeley, Berkeley, CA 94720

[4]NASA Goddard Space Flight Center, Greenbelt, MD, 20771

[5]Science Systems & Applications, Inc.

Gamma-ray lines from the inelastic interactions of accelerated ions with ambient nuclei in solar flares (Lingenfelter & Ramaty 1967) were first observed by Chupp et al. (1973). Since the de-excitation lines are generally emitted in much less than a microsecond, they are Doppler-shifted according to the recoil velocity of the emitting nucleus immediately after the original interaction, which in turn preserves some of the information of the initial velocity of the exciting ion. Accelerated protons and α-particles produce lines narrow enough to be easily separated from the continuum. Ramaty and Crannell (1976) discussed the use of the profile of the de-excitation lines as a means of finding the angular distribution of the accelerated particles. Computer codes now generate predicted line profiles and fluxes given the energy and angular distributions of the accelerated ions and the compositions of the accelerated and ambient populations (Ramaty, Kozlovsky & Lingenfelter 1979; Murphy, Kozlovsky & Ramaty 1988; Kiener, de Séréville, & Tatischeff 2001; Share et al. 2002; Kozlovsky, Murphy & Ramaty 2002). These codes were recently applied to an ensemble of gamma-ray line flares from the *Solar Maximum Mission* Gamma-Ray Spectrometer (*SMM*) (Share et al. 2002). Share et al. (2002) found that narrow lines exhibit $\sim 1\%$ redshift for flares at small heliocentric angles, but are not shifted near the limb of the Sun. Their measurements were consistent with a downward isotropic distribution of accelerated particles, i.e. one corresponding to significant pitch angle scattering in the corona.

Although the *SMM* data yielded useful measurements of some nuclear-line redshifts and put some constraints on the line widths, the energy resolution of that instrument was moderate, averaging around 4% FWHM over the nuclear-line range. The desire for high-resolution measurements of the shape and redshift of de-excitation lines was one of the main motivations for the design of *RHESSI* (Lin et al. 2002, 2003). *RHESSI* uses cryogenically cooled germanium detectors to achieve an energy resolution averaging around 0.2% FWHM from 1–6 MeV (Smith et al. 2002).

2. Analysis and Results

The spectrum presented here uses the thick rear segments of the *RHESSI* germanium detectors, which have most of the efficiency for stopping gamma-rays above 300 keV(Smith et al. 2002). Detector #2, which is operated in an unsegmented mode and has degraded energy resolution, was not used. The energy range from 3084–3226 keV was excluded from spectral fitting due to a known instrumental artifact in the spectra, and one detector (#5) was excluded in the range 1570–1605 keV due to another artifact peculiar to it (see Smith et al. (2002) for details).

The spectra shown in Figure 1 were accumulated from 00:27:30 to 00:43:30 UT on 23

July, 2002, an interval that includes most of the high-energy emission from this flare (Lin et al. 2003). The instrumental background was determined by accumulating two spectra of the same duration as the flare from 15 orbits (approximately one day) before and after it. This method assures that the parameters that control the background have nearly the same values as during the flare. Above 3 MeV the background is simple in form and nearly free of lines, so we could accumulate a full day of data for the background to reduce statistical fluctuations, rescaling it to match the intensity of the background generated at ±15 orbits.

The full spectrum is shown in Lin et al. (2003). Fits to the six most significant nuclear de-excitation lines are shown in Table 1, and the spectra are shown in Figure 1. The full spectrum from 250 keV to 8.5 MeV was fitted with these lines plus a broken power-law representing electron bremsstrahlung (the index hardens from 2.77 to 2.23 at a break energy of 617 keV), three very broad Gaussians centered at 1845, 4358 and 6575 keV, and the delayed lines from positron annihilation and neutron capture (511 keV and 2223 keV, respectively). The broad Gaussians substitute for the sum of the broad lines from interactions of accelerated heavy ions with ambient hydrogen and the ensemble of low-level narrow lines (mostly around 1–2 MeV) that are too faint to measure individually. The fitting was done with the Spectral Executive (SPEX) package (Schwartz 1996), taking into account the full off-diagonal response of the instrument (Smith et al. 2002). The unreduced χ^2 was 809 for 732 degrees of freedom; the probability of this value or higher is 2.5% if the model is sufficient.

The sum of the fluences in the narrow lines of Table 1 is 138 ph cm^{-2}. Share & Murphy (1995) calculated the total fluence in narrow lines for 19 X-class flares observed by *SMM*. They included several fainter lines that we do not detect with comparable significance to those in Table 1. Estimating the contribution of these lines to the 23 July flare by their average contribution in the flares studied by Share & Murphy (1995) gives a total fluence of

Table 1. Best fit Gaussian parameters for prompt nuclear lines

Isotope	Rest Energy (keV)	Fit Energy (keV)	% Redshift	FWHM (keV)	% FWHM	Flux ($\times 10^{-2}$ ph cm^{-2} s^{-1})	*SMM* % Redshift	*SMM* % FWHM
^{56}Fe	847	$846.2^{+0.7}_{-0.7}$	$0.10^{+0.08}_{-0.08}$	$2.9^{+1.9}_{-1.9}$	$0.34^{+0.22}_{-0.22}$	$1.08^{+0.30}_{-0.30}$	...	...
^{24}Mg	1369	$1363.7^{+1.8}_{-2.0}$	$0.39^{+0.13}_{-0.14}$	$17.2^{+6.1}_{-4.1}$	$1.25^{+0.45}_{-0.30}$	$2.27^{+0.71}_{-0.59}$	...	...
^{20}Ne	1634	$1628.7^{+1.7}_{-1.7}$	$0.32^{+0.10}_{-0.10}$	$15.5^{+3.6}_{-3.0}$	$0.95^{+0.22}_{-0.18}$	$1.84^{+0.36}_{-0.35}$	0.0 ± 0.2	2.9 ± 1.0
^{28}Si	1779	$1776.7^{+1.9}_{-1.9}$	$0.13^{+0.11}_{-0.10}$	$14.4^{+5.8}_{-5.3}$	$0.81^{+0.33}_{-0.30}$	$1.56^{+0.52}_{-0.45}$	...	...
^{12}C	4438	$4400.7^{+11.1}_{-11.7}$	$0.84^{+0.25}_{-0.26}$	$95.4^{+36.0}_{-26.8}$	$2.15^{+0.81}_{-0.60}$	$3.24^{+1.07}_{-0.98}$	-0.07 ± 0.14	3.18 ± 0.74
^{16}O	6129	$6081.7^{+11.9}_{-13.3}$	$0.77^{+0.19}_{-0.22}$	$151.3^{+63.8}_{-35.9}$	$2.47^{+1.04}_{-0.59}$	$4.35^{+0.47}_{-0.46}$	-0.26 ± 0.13	...

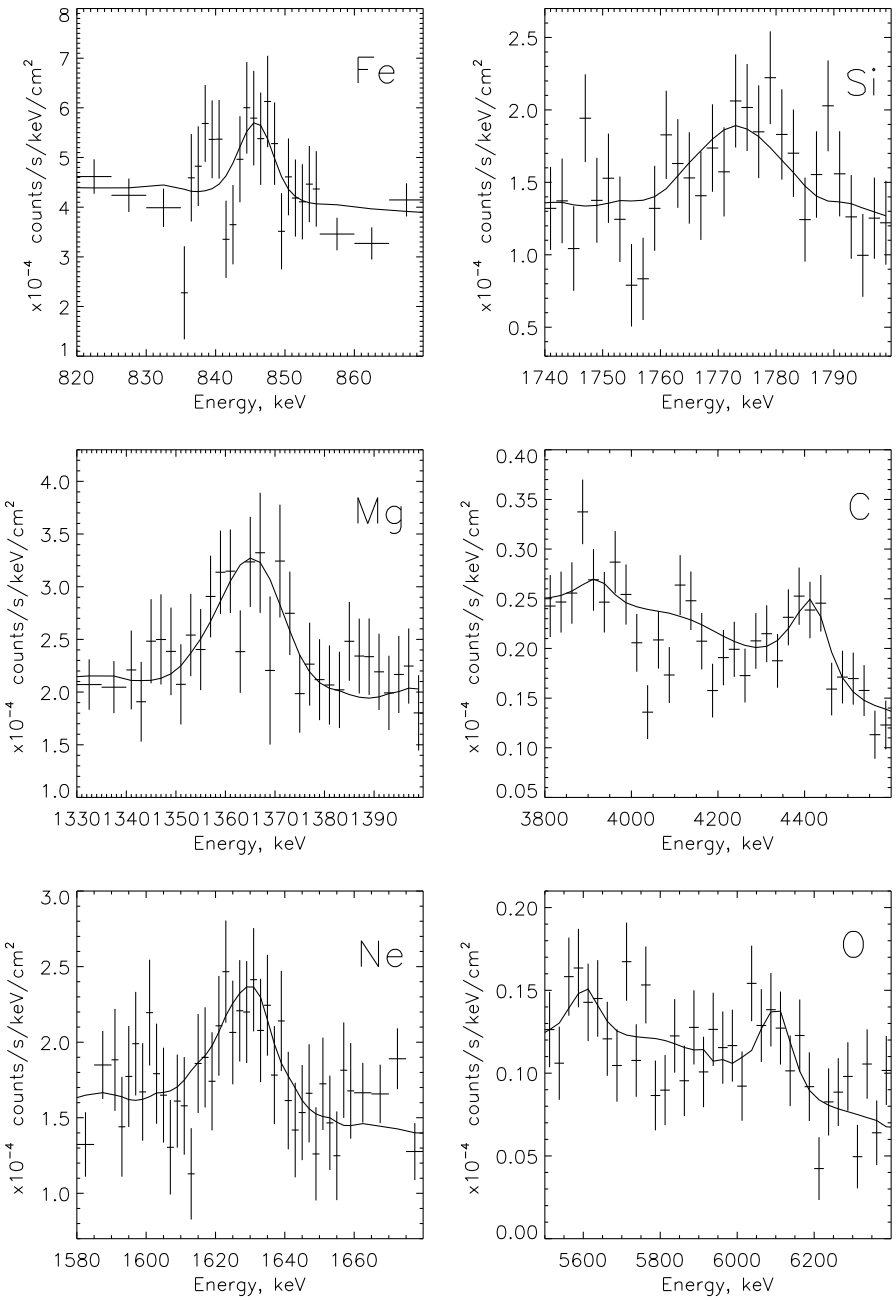

Fig. 1.— *RHESSI* background-subtracted count spectra from 00:27:20 UT to 00:43:20 UT on 23 July, 2002. Each panel is labeled with the element primarily responsible for the line shown. The fits to the carbon and oxygen lines include the single annihilation-line escape peak, which also contains information on the line shape. The fit shown in each panel is for λ=20, S=2.75, R=0.6, and θ=0 (see text).

about 180 ph cm^{-2}. The *SMM*flares have a bimodal distribution in intensity with 13 events from 16–55 ph cm^{-2} and six from 108.5–293.8 ph cm^{-2}. Neither the GOES class nor the heliocentric angle correlates with the line fluence in that data set. The 23 July flare falls squarely into the category of line-bright events, which includes flares of GOES class X2.8 to X15.0.

Table 1 shows that the percentage redshift and width of the lines is inversely related to the nuclear mass, as is expected for recoil. The last two columns of the table show results from Share et al. (2002) for the average of five flares close to a heliocentric angle of 74^{o}. There is no observable redshift and the line widths are higher. The advantage of a high-resolution instrument is clear: the *RHESSI* results are more complete using a single flare, even though *RHESSI's* effective collecting area is considerably smaller than *SMM's*. With more flares observed at high resolution, we will be able to tell whether the differences are due to intrinsic variations between flares or to the limitations of *SMM's*moderate-resolution spectroscopy.

3. Modeling and Discussion

The cross-section versus energy for stimulation of each nuclear line has a sharp lower boundary, rising rapidly to a peak and then falling off gradually (Kozlovsky, Murphy & Ramaty 2002). When these cross-sections are convolved with a falling spectrum of interacting particles, the result is that each line is stimulated mainly by protons or α-particles in a very narrow ranges of energies, almost independent of the spectral index. Because of the greater recoil, the α-induced component of each line is more Doppler-broadened and has a higher redshift. The α-induced cross sections peak at lower energies per nucleon, so the ratio of the α- and proton-induced components of each line is a function of both the α/proton ratio in the accelerated particles and their spectral index. For a single line, then these two parameters cannot be separately constrained, but this degeneracy is broken by considering multiple lines, since the ratio between the threshold energies for α-particles and protons varies.

The modeling code (Murphy, Kozlovsky & Ramaty 1988) allows an arbitrary angular distribution of incident particles about an axis at an arbitrary angle to the observer (θ). For particles distributed with respect to a field line perpendicular to the Sun, θ is equal to the heliocentric angle, 73^{o} for this flare. The code generates separate line spectra due to energetic α-particles and protons, with line shapes including the effects of nuclear recoil both from the inelastic collision and the emission of the gamma ray. Thus even a purely downward beam of incident protons gives broadened lines due to the range of recoil angles.

We ran simulations for spectral indices S of 1.75, 2.75, 3.75, 4.75, and 5.75, assuming the protons and α-particles have the same index. Angular distributions representing strong, intermediate and negligible pitch-angle scattering had values of λ = 20, 300, and 10000, where λ is the scattering mean free path divided by the half-length of the coronal segment of the magnetic loop (Hua et al. 1989; Murphy et al. 1990; Share et al. 2002). A pure downward beam and a distribution isotropic in the downward hemisphere were also run. The $\lambda = 10000$ case gives a fan beam (peaked around 90° to the field line) with no net redshift, and is ruled out by the data. For each case, the magnetic field angle to the line of sight, θ, was run at 0°, 30°, 45°, 52°, 60°, 73°, and 80°.

For each of these models, we tried summing the proton- and α-induced components for α/proton ratios R (at the same energy per nucleon) from 0.01 to 2.00 in steps of 0.01. The models were then folded through the instrument response and compared to the data, re-fitting the flux in each line separately. The spectral components other than the six de-excitation lines under consideration had their values fixed to those generated in the fit that produced Table 1. Figure 3 shows contours of $\chi^2_{min} + 1.00$, $\chi^2_{min} + 2.71$, and $\chi^2_{min} + 7.78$, which represent respectively a 68% and 90% chance of enclosing the correct value of a single parameter of interest and a 90% chance of enclosing the correct value of all four parameters (Lampton, Margon & Bowyer 1976). Plots are shown for strong pitch-angle scattering (λ = 20, which is nearly identical to the result for a downward isotropic distribution) and a downward beam. For $\lambda = 300$, there is only a $\chi^2_{min} + 7.78$ contour (restricted to $\theta < 30°$), and $\lambda = 10000$ is completely ruled out even at that level.

The most striking overall result is that the heliocentric angle of 73° is clearly excluded for θ for any of the pitch-angle-scattering (λ) models. The redshifts are large enough that either the field lines in the loop legs must be significantly bent toward us instead of being perpendicular to the solar surface, or else the pitch angle distribution is strongly beamed downwards, whether due to the influence of strong parallel electric fields or another phenomenon. If, in general, the magnetic loops containing accelerated ions are often bent from the perpendicular, it may explain the discrepancy between our line widths in Table 1 and the systematically broader lines found by Share et al. (2002) using *SMM*. They combined multiple flares in the same range of heliocentric angle before making spectral fits. It is possible that the flares in each of their samples had a wider range of θ than of heliocentric angle, and therefore different redshifts were combined to make broader lines in the composite spectra.

The decay rate of the neutron capture line at 2.223 MeV in this flare (Murphy et al. 2003) favors models with λ in the range of 200–2000 and rejects a downward-beamed distribution with 90% confidence except in the case of an extremely low ambient ^{3}He abundance. An isotropic distribution of accelerated α-particles was also strongly favored over a downward

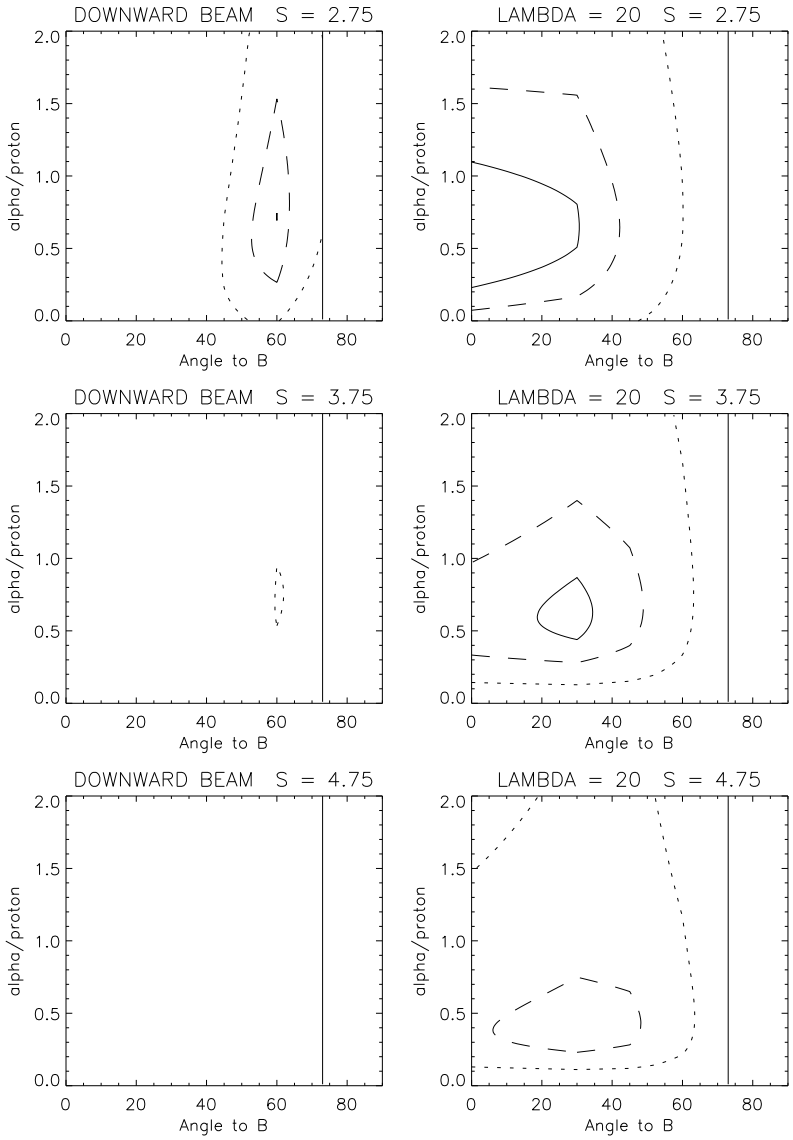

Fig. 2.— Contours of constant $\Delta\chi^2$ beyond the minimum value. Solid lines are $\chi^2_{min} + 1.00$, dashed lines are $\chi^2_{min} + 2.71$, and dotted lines are $\chi^2_{min} + 7.78$. The vertical line at 73° is the heliocentric angle of the flare.

beam in an *SMM* study of the combined lines at 0.429 and 0.478 MeV from α-α reactions (Share & Murphy 1997). The low redshifts of the ^{20}Ne, ^{12}C and ^{16}O lines in multiple flares seen by *SMM* (Share et al. 2002) favored a downward isotropic distribution (or one with a slight additional upward component) to a downward beam. The lack of redshifts seen in Table 1 for the *SMM* flares near 74^{o} heliocentric angle are part of that result. Although the preponderance of external evidence thus seems to favor a bent loop over a downward-beamed distribution to explain the high redshifts we see in this flare, a conclusive result awaits further observations of gamma-ray lines at high resolution.

The overall constraint on R is weak: values all the way from 0.1 to 2.0 are allowed within the 90% confidence interval, although values near 0.6 are preferred, consistent with the number deduced from flux measurements by *SMM* and *CGRO* of lines induced only by α-particles (Share & Murphy 1998). The spectral index S is also poorly constrained, although 2.75 is favored as can be seen in Figure 2. But this is the first demonstration that these parameters can be constrained at all using only the shapes of the lines. The full power of the spectral analysis of gamma-ray lines will be realized when these constraints are combined with information from the gamma-ray line fluxes and from other observations such as gamma-ray and x-ray imaging (Hurford et al. 2003), magnetograms and imaging at other wavelengths, and temporal observations such as the decay rate of the neutron capture line (Murphy et al. 2003).

This work was supported by NASA contract ?????????.

REFERENCES

Chupp, E. L., Forrest, D. J., Higbie, P. R., Suri, A. N., Tsai, C., & Dunphy, P. P. 1973, Nature, 241, 333

Hua, X.-M., Ramaty, R., & Lingenfelter, R. E. 1989, ApJ, 341, 516

Hurford, G. et al. 2003, ApJ, this issue

Kiener, J., de Séréville, N., & Tatischeff, V. 2001, Phys. Rev. C., 64, 025803

Kozlovsky, B., Murphy, R. J., & Ramaty, R. 2002, ApJ, 141, 523

Lampton, M., Margon, B., & Bowyer, S. 1976, ApJ, 208, 177

Lin, R. P. et al. 2002, Solar Physics, in press

Lin, R. P. et al. 2003, ApJ, this issue

Lingenfelter, R. E. & Ramaty, R. 1967, in High Energy Nuclear Reactions in Astrophysics, ed. B. S. P. Shen (New York: W. A. Benjamin), p. 99.

Murphy, R. J., Kozlovsky, B., & Ramaty R. 1988, ApJ, 331, 1029

Murphy, R. J., Hua, X.-M., Kozlovsky, B., & Ramaty R. 1990, ApJ, 351, 299

Murphy, R. J., Share, G. H., Hua, X.-M., Lin, R. P., Smith, D. M., & Schwartz, R. A. 2003, ApJ, this issue

Ramaty, R. and Crannell, C. J. 1976, ApJ, 203, 766

Ramaty, R., Kozlovsky, B., & Lingenfelter, R. E. 1979, ApJS, 40, 487

Schwartz, R. A. 1996, "Compton Gamma Ray Observatory Phase 4 Guest Investigator Program: Solar Flare Hard X-ray Spectroscopy," Technical Report, NASA Goddard Space Flight Center

Share, G. H. & Murphy, R. J. 1995, ApJ, 452, 933

Share, G. H. & Murphy, R. J. 1997, ApJ, 485, 409

Share, G. H. & Murphy, R. J. 1998, ApJ, 508, 876

Share, G. H., Murphy, R. J., Kiener, J., & de Séréville, N. 2002, ApJ, 573, 464

Smith, D. M. et al. 2002, Solar Physics, in press